Electron transfer from H_2 and Ar to stored multiply charged argon ions produced by synchrotron radiation

S. D. Kravis* and D. A. Church
Physics Department, Texas A&M University, College Station, Texas 77843

B. M. Johnson, M. Meron, and K. W. Jones
Department of Applied Science, Brookhaven National Laboratory, Upton, New York 11973

J. C. Levin and I. A. Sellin
Physics Department, University of Tennessee, Knoxville, Tennessee 37996
and Oak Ridge National Laboratory, Oak Ridge, Tennessee 37831

Y. Azuma, N. Berrah-Mansour, and H. G. Berry
Physics Division, Argonne National Laboratory, Argonne, Illinois 60439

M. Druetta
Laboratoire Traitement du Signal et Instrumentation, Université de St. Etienne, St. Etienne, France
(Received 8 November 1991)

The rate coefficients for electron transfer from Ar and H_2 to Ar^{q+} ions ($3 \le q \le 6$) have been measured using an ion-storage technique in a Penning ion trap. The ions were produced in the trap by K-shell photoionization of Ar atoms, using broadband synchrotron x-ray radiation. K-electron removal resulted in vacancy cascading, yielding a distribution of argon-ion charge states peaked near Ar^{4+}. The stored ion gas had an initial temperature near 480 K. The basic data determining the rate coefficients $k(Ar^{q+})$ are the storage time constants of each charge state in the trap, in the presence of a measured pressure of target gas. The results of the measurements (in units of 10^{-9} $cm^3 s^{-1}$) are $k(Ar^{3+},H_2)=4.3(0.7)$, $k(Ar^{3+},Ar)=1.6(0.2)$, $k(Ar^{4+},H_2)=5.2(0.6)$, $k(Ar^{4+},Ar)=2.5(0.3)$, $k(Ar^{5+},H_2)=5.9(0.7)$, $k(Ar^{5+},Ar)=2.9(0.3)$, $k(Ar^{6+},H_2)=8.5(1.2)$, and $k(Ar^{6+},Ar)=2.5(0.3)$.

PACS number(s): 34.70.+e, 32.80.Hd, 82.30.Fi

I. INTRODUCTION

The rate coefficients or cross sections for charge-changing collisions of low-energy multiply charged ions are required for a detailed understanding of important collision-related processes in astrophysical plasmas [1], as well as in laboratory plasmas used for fusion research [2], and for certain types of potential x-ray lasers. The measurements reported here were essential in the analysis of studies of the inner-shell photoionization of an Ar^{2+} target [3,4], also stored in a Penning ion trap. Except for collisions of He and Ne with doubly charged ions of the lanthanide series, La^{2+}, Ce^{2+}, etc., the ionization potentials of multiply charged ions greatly exceed those of atoms or molecules with which they collide, so electron transfer from the neutral to the ion is energetically favored. Electrons are captured typically into excited states of the ion, generally resulting in the radiation of energy from the plasma. The identities of the states which are populated depend on the details of the potential surfaces of the multicharged pseudomolecule temporarily formed during the collision, and on the relative velocities of the collision partners. As the internuclear distance changes during the collision, an electron is transferred near avoided crossings of the pseudopotential surfaces. Thus the cross sections depend critically on the energies of the final states, and can have significant velocity dependences in the low-energy region. No general theoretical scaling of cross sections calculated quantum mechanically is feasible [5]. Since the use of approximations to calculate particular cross sections or rate coefficients is essential, the availability of measurements is useful to theory, particularly at the lowest collision energies where the theory is best defined.

In recent years a number of measurements of rate coefficients for electron transfer to multiply charged ions have been described [6–10]. However, the methods employed for ion production in the measurements reported here, and the consequences of these new methods, are novel. Briefly, a distribution of multicharged argon-ion charge states was produced in a Penning ion trap by K-shell photoionization of argon using synchrotron radiation [11]. The stored ions had a thermal distribution characterized by a mean temperature near 480 K. Each charge state captured electrons from the target gas, either H_2 or Ar in this case, leading to storage for a characteristic time in the trap. The rate coefficients for electron transfer were computed from the measured target-gas density and characteristic storage time constants. Because of the simultaneous storage of several charge states, and the possibility of ions remaining in the trap following electron transfer, a detailed analysis of the rate coefficient

determination is described, based on the properties of the stored ion cloud.

The Penning trap [12] combines static electric and magnetic fields to confine the ions. The electrode configuration creates an axially symmetric quadrupole electrostatic potential which confines positive ions axially, but defocuses positive ions radially, when the end-cap electrodes are biased positive relative to the ring electrode. The ions are prevented from escaping radially by introducing a uniform magnetic field in the z direction. The axial magnetic field and the radial electric field together cause an $\mathbf{E}\times\mathbf{B}$ drift of the ions about the trap symmetry axis.

The quadrupole potential of the trap is given by

$$V=\left[\frac{V_0}{r_0^2+2z_0^2}\right][2(z^2-z_0^2)-x^2-y^2] \tag{1}$$

and the equation of motion for an ion is

$$m\mathbf{v}=-q\nabla V(r)+(q\mathbf{v}\times\mathbf{B}) . \tag{2}$$

Solving the equations of motion, the ions have three characteristic oscillatory frequencies: ω_z in the z direction and ω_+ and ω_- in the x-y plane. ω_- is interpreted as the frequency of the $\mathbf{E}\times\mathbf{B}$ drift about the trap symmetry axis and ω_+ is the cyclotron frequency altered slightly by the $\mathbf{E}\times\mathbf{B}$ drift. In most situations it is found that $\omega_+ \gg \omega_z \gg \omega_-$. With this in mind $\omega_- \approx \omega_z^2/2\omega_C$ and $\omega_+ \approx \omega_C - \omega_-$, where ω_+ and ω_- are given by

$$\omega_+=\frac{\omega_C}{2}+\omega_0 , \tag{3}$$

$$\omega_-=\frac{\omega_C}{2}-\omega_0 , \tag{4}$$

$$\omega_0=\left[\frac{\omega_C^2}{4}-\frac{\omega_z^2}{2}\right]^{1/2} . \tag{5}$$

In order to have a bounded solution ω_0 must be real, that is,

$$\frac{\omega_C^2}{4}\geq\frac{\omega_z^2}{2} \tag{6}$$

and in terms of ion stability for a given magnetic field

$$B\geq\left[\frac{2mV_0}{qz_0^2}\right]^{1/2} . \tag{7}$$

For these rate coefficient measurements the initial ion cloud was formed by synchrotron radiation transmitted through slits in the segmented ring electrode rather than through the end-cap electrodes. There have not been extensive studies of the ion temperature and evolution for this form of ion production.

II. APPARATUS

The Penning trap (see Fig. 1) was designed to accept a 1.4-cm-wide fan of unfocused synchrotron radiation (SR) through the radial plane at the minimum of the axial potential well. The magnetic field of the trap was provided

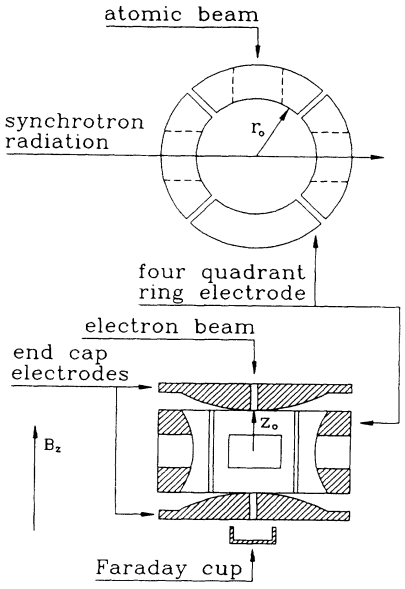

FIG. 1. Top: the four-quadrant ring of the Penning ion trap, with the direction of the synchrotron-radiation beam indicated. The pulsed atom beam was not used in the rate coefficient measurements. Bottom: a section of the trap structure, showing the electron beam apertures and Faraday cup used for trap alignment in the magnetic field, and synchrotron beam centering in the trap.

by an electromagnet with 6-in.-diam pole tips separated by a 2-in. gap. The field was oriented vertically. The magnet power supply provided currents to produce fields up to 0.8 T. The trap electrodes were a spherical approximation to the ideal hyperboloids of revolution, with a ring electrode radius $r_0=10.8$ mm and an end-cap separation $2z_0=15.2$ mm. The ring electrode was divided into quadrants. Two of these opposing quadrants had rectangular apertures 3 mm high by 1.4 cm wide, to transmit the synchrotron radiation, and one of the remaining quadrants had a similar aperture to easily admit target gas from a nearby gas pulsing source used for other measurements [3,4,13]. Each end cap had a 1.3-mm-diam central hole, to transmit electrons from an attached electron source, parallel to the magnetic field lines, through the trap to a Faraday cup attached to the other end cap. Ions created by electron impact were used for diagnostic purposes and other measurements.

The SR beamline contained three features that affected the SR: a 1:1 focusing mirror, two Be windows, and a mechanical beam chopper. The 1:1 focusing mirror [14] located 10 m from the source accepted 4 mrad of the horizontal fan of SR and focused it 20 m from the source. The mirror substrate was 60 cm long and made of zerodur. A 4-cm-wide cylindrical channel was cut, polished, and coated with platinum. Characterization of the mirror was performed by using a Si(Li) x-ray detector positioned at a forward scattering angle of 45° to measure photons scattered through air after passage through a 20×20 μm^2 pinhole. The SR spot size at the mirror

focus had a FWHM of 0.7 mm in the horizontal direction and 0.6 mm in the vertical direction [15]. Without the mirror the SR profile would have been 8 cm wide and 1.8 mm high had there been no limiting apertures. The focusing in the vertical direction is due to a slight concave curvature along the axis of the cylindrical surface of the mirror.

One Be window separated the beamline vacuum from the storage ring vacuum and another Be window separated the experimental vacuum chamber from the beamline vacuum. The effect of the Be windows on the SR was to sharply attenuate photons with energies less than 3 keV.

Ar has a K-shell binding energy near 3.2 keV. This suggests that primarily K-shell ionization will occur since the Be windows sharply attenuate photons with energies less than 3 keV. For photon energies greater than the K edge, the relative probability of a K, L, or M-shell ionization is approximately 0.9, 0.09, and 0.01, respectively [15]. A mechanical beam chopper made of tantalum was located 17 meters from the source. The chopper was used to temporarily block the SR during ion storage intervals. The chopper took about 3 ms to go from the fully blocked (unblocked) to the fully unblocked (blocked) positions. The SR exited the experimental apparatus through a third beryllium window and passed through an ion chamber used to calibrate the relative SR intensity.

The trap and the focused SR beam were aligned by the following procedure. The trap vacuum chamber was filled to ≈ 10 mTorr of Ar. The focused SR was allowed to pass through the trap while the magnetic field was on and the end-cap electrodes were biased positive relative to the ring electrode. The ejected electrons from the photoionized Ar followed the magnetic and electric field lines to the end-cap electrodes. When the SR passed through the trap axis, the electrons could pass through the holes in the centers of the end-cap electrodes, and one-half of them would be collected by the Faraday cup (see Fig. 1). The trap and magnet were simultaneously translated perpendicular to the photon beam while the photoelectron current was measured. The peak in the photoelectron current indicated that the SR beam was passing over the centers of the end-cap electrodes. A Gaussian beam profile was convoluted with the holes in the end-cap electrodes to obtain a full width at half maximum (FWHM) for the SR beam at the center of the trap of 1.7 mm. This indicates that the center of the trap was approximately 40 cm from the focal spot of the SR. The difference in this measurement and the one described above which gave a FWHM of 0.7 mm is reasonable. The cumbersome apparatus may have not been placed at the exact focus of the SR, and once the apparatus was in place the SR beam was steered through the trap by adjusting the mirror. The adjustment could change the focal point position slightly. The vacuum system consisted of pumps, gauges, gas inlets, and a tube to the ion trap, all mounted on a six-way cross. Before the measurements, the vacuum system was baked at just over 100 °C, while being evacuated with a 250-l/s ion pump. It was observed that when pumping argon the ion pump emitted certain other gases previously adsorbed, so during the rate measurements, the ion pump was shut off and only the cryopump and sorption pump on the six-way cross were used to evacuate the system. A nude ion gauge (NIG) and residual gas analyzer (RGA) were mounted at the same position relative to the active pumps as the ion trap and target-gas inlet, so the gauge readings were not systematically affected by a pressure gradient. Further, a 150-l/s cryopump mounted between the trap and the upbeam Be window was valved off to eliminate the possibility of a pressure gradient through the tube leading to the trap associated with gas flow produced by pumping at both ends of the tube. However, a pressure gradient between the trap and the pumps due to residual gases evolved from the walls of the vacuum system near the trap is thought to have existed. The uncalibrated RGA indicated that H_2 was the dominant residual gas in the system near base pressure ($\leq 10^{-9}$ Torr), with some CO or N_2 and water vapor also indicated. At the lowest H_2 target-gas pressure used in the measurements, residual gases were less than 3% of the H_2 partial pressure. Densities of H_2 target gas described in the measurements were computed using the calibrated NIG readings, corrected for the gauge factor and for a small systematic gauge reading error obtained by linear extrapolation of the pressure calibration to the operating pressures.

For the Ar^{q+} on H_2 measurement a slow leak of argon gas was admitted into the vacuum system along with a much larger leak of H_2. The argon pressure was maintained at 5×10^{-9} Torr while the H_2 pressure was varied from 2×10^{-8} to 7×10^{-8} Torr. A tee was connected to a port on the vacuum chamber with shutoff valves and needle valves connected to argon and H_2 reservoirs on each arm. The H_2 pressure was regulated by placing an MKS 248A control valve between the H_2 bottle and the reservoir. The valve was operated in the pressure control mode by the valve controller. It was necessary to regulate the H_2 pressure because the high flow rate of H_2 from the reservoir to the trap vacuum would otherwise rapidly deplete the reservoir of H_2.

Experimental control and data acquisition was accomplished with an IBM XT–compatible computer and an array of custom electronics modules. Figure 2 is a schematic of the experimental setup.

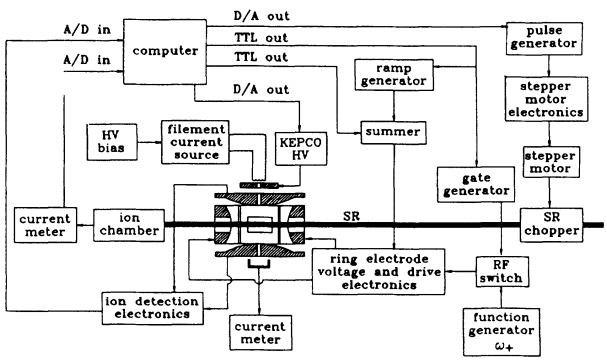

FIG. 2. A schematic diagram of the ion trap and electronics, including axial ion detection, radial excitation at ω_+, and the synchrotron beam chopper, with computer control and data collection. SR denotes "synchrotron radiation."

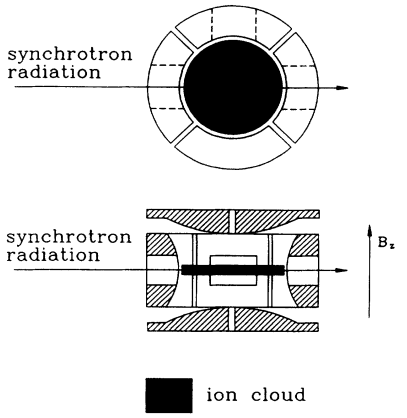

FIG. 3. A schematic view of the ion cloud distribution formed by photoionization of neutrals in the trap. The ion cloud density peaks at the trap center, and decreases radially, due to the magnetron rotation of the ions.

The ions were detected using the resonant tuned circuit method for axial oscillation detection [16]. An inductor was connected across the trap end-cap electrodes which produced the capacitance of the tuned circuit. Radio frequency at the resonance frequency of the circuit was applied and the ring voltage was ramped, successively forcing ions of different mass-to-charge ratio m/q to be resonantly excited. This modulated the applied rf. The modulated rf was then amplified and demodulated to obtain a spectrum of modulation peaks versus voltage. The ions were initially formed at a trap ring electrode potential of -1.5 eV, which was ramped to -15 V for ion detection. A digital output from the computer triggered a ramp generator module. A second digital pulse was generated by the computer after the ramp and added to the ramp voltage by a summing module. This made the ring voltage greater than 0 V to throw out any remaining ions in the trap after each acquisition cycle. Ions were initially formed in the path of the SR, across the diameter of the trap. The ions precess about the symmetry axis with a frequency near ω_- due to the $\mathbf{E}\times\mathbf{B}$ drift, forming a pancake-shaped ion cloud (see Fig. 3) at the potential minimum of the trap.

III. ION ENERGY DETERMINATION

Using geometric considerations, the initial ion density as a function of r, when neglecting charge capture, is

$$\rho=\rho_{\rm sp} \quad \text{for } r<r_{\rm sp} \tag{8}$$

$$\rho=\frac{G\rho_{\rm Ar}t}{\pi r\sigma_z} \quad \text{for } r>r_{\rm sp} \ . \tag{9}$$

For $r<r_{\rm sp}$ the density would be constant and at maximum equal to the space charge limited density [16] $\rho_{\rm sp}$. G is the integral of the photoionization cross section and the photon flux as a function of energy $\int f(E)\sigma(E)dE$ calculated to be 2.8×10^{-4} photons cm^2 s^{-1} when including the focusing effects of the mirror and assuming a mean synchrotron ring current of 140 mA. $\rho_{\rm Ar}$ is the neutral argon density, t is the time of ionization, and σ_z is the vertical height of the synchrotron radiation beam. It should be noted that Eq. (9) applies only for the ion production since ion-ion and ion-neutral collisions can redistribute the ions. The SR produced a stored distribution of charge states ranging from Ar^{2+} to Ar^{8+}, peaking at the charge state 4+. The Ar partial pressure was 5×10^{-9} Torr during the rate measurements with the H_2 target.

The maximum Ar^{4+} ion density in the trap during measurements was estimated to be 5×10^5 cm^{-3}. Using this density and the estimated mean ion temperature, the equilibration time constant due to Coulomb collisions between ions with different charge was about 10 ms, and the Debye length near 6 mm [11]. Thus the Debye length was less than the diameter of the stored ion cloud, but still larger than the axial height of the cloud. This situation could lead to some migration of ions with different charge states within the ion cloud, with the lower-charged ions moving to larger radius. This does not affect the rate coefficient measurements directly, but could affect the storage of product ions in the trap.

Precise alignment of the SR beam in the vertical (trap axis) direction was not carried out for practical reasons. The SR beam center could have been as much as 0.6 mm away from the center of the trap in the vertical direction. The kinetic energy of an ion due to the axial motion is $E_z=m\omega_z^2z^2/2$ and the Gaussian profile of the SR has the form

$$f(z)=(1/2\pi\sigma^2)^{1/2}\exp[-(z-z_C)^2/2\sigma_z^2] \ .$$

z_C is the displacement of the center of the beam from the center of the trap on the vertical axis and σ_z is $(4\ln2)^{-1}$ FWHM. From this we find the average axial energy of the ions to be

$$\langle E_z\rangle=\tfrac{1}{2}m\omega_z^2\sigma_z^2\left[\frac{z_C^2}{\sigma_z^2}+1\right] \ . \tag{10}$$

If the SR is centered vertically so $z_C=0$, then $\langle E_z\rangle=2.4$ meV. If the beam is off center by one FWHM then $\langle E_z\rangle=21$ meV.

To find the total mean kinetic energy of the ions, the initial mean energy of the target neutral atoms and the kinetic energy in the magnetron motion must be added. The initial energy is distributed in the axial and cyclotron motions, depending on the direction the target atom is traveling at the moment of ionization. The initial energy of the atoms is taken as room temperature (≈300 K). The average magnetron energy was $\langle E_-\rangle=(\frac{1}{2})m\omega_-^2\langle r\rangle^2=1.7$ meV. Adding all the contributions together, the average energy of a stored ion is between 43 and 62 meV. Evaporative cooling [16] of the stored ions does not take place since the energy of the ions when formed is already more than an order of magnitude smaller than the well energy qD.

IV. PROCEDURE AND RESULTS

A distribution of charge states ($2\le q\le8$), created by a 1-s SR pulse through the trap ring electrodes, was stored.

Charge states 7+ and 8+ were produced in quantities too small ($\approx 3\%$ of the total distribution) for accurate rate coefficient measurements. The ions were stored for a preset amount of time with the SR blocked by the mechanical chopper. The trap ring voltage was -1.5 V relative to that of the end caps during the storage time, so the well depth D was 0.75 V. During this storage interval, the ions go through charge exchanging collisions with H_2 and Ar which modify the ion charge distribution. After this storage interval the ions were detected as previously described. To get a good signal-to-noise ratio (S/N), 100 to 500 cycles were added together depending on the ion numbers, storage times, and H_2 pressure.

The storage time was varied so that decay curves for each charge state could be made to determine the $1/e$ time constants τ_i. The H_2 partial pressure was then changed to get families of decay curves for different pressures. Figure 4 shows decay curves for Ar^{5+} at three different H_2 pressures, relative to the fixed argon pressure. Similar curves were obtained for the other charge states (see Fig. 5). A plot of $1/\tau$ versus H_2 density is expected to yield a straight line with a slope equal to the charge-capture rate coefficient. A similar procedure with only Ar target gas was used to obtain the rates for collisions with argon.

In fact, the rate coefficients were not found so easily. Two other processes occurred that altered the decay curves from being purely the result of ion loss due to charge capture from H_2. Besides charge capture from H_2 the argon ions can react with the argon gas that was leaked into the ion trap vacuum chamber as the target for the SR. This contributes to the intercept of the $1/\tau$ versus density plot at zero H_2 density. Secondly, when an Ar^{q+} ion captures an electron, it becomes an $Ar^{(q-1)+}$ ion that has some probability of remaining in the trap. Using geometric and energy considerations, the fraction of ions that leave the trap after capturing a single electron is

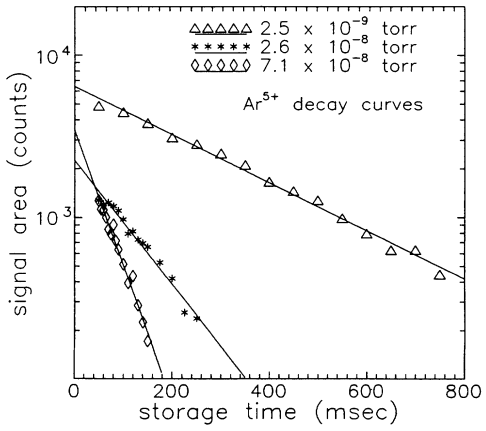

FIG. 4. The decrease in stored Ar^{5+} number with storage time in the trap, at three different pressures of H_2 target gas. The argon production gas pressure was 5×10^{-9} Torr for all measurements.

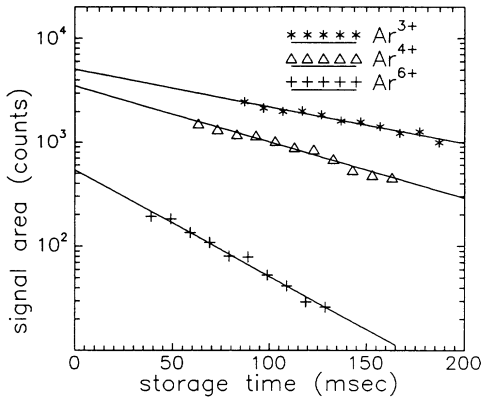

FIG. 5. Representative stored ion number vs storage time in the trap for Ar^{3+}, Ar^{4+}, and Ar^{6+} ions at an H_2 target-gas pressure of 6×10^{-8} Torr.

$$f_{\text{loss}}=1-\left[\frac{E_{\text{es}}}{E_I}\right]^{1/2} \tag{11}$$

and the fraction of ions retained in this process is

$$f_{\text{ret}}=\left[\frac{E_{\text{es}}}{E_I}\right]^{1/2}, \tag{12}$$

where E_{es} is the energy necessary for the ion of original charge q to escape the trap axially. This is given by

$$E_{\text{es}}=(q-1)eV$$
$$=(q-1)e\frac{V_0}{r_0^2+2z_0^2}[2(z^2-z_0^2)-x^2-y^2]\,. \tag{13}$$

E_I is the energy of the ion gained by the Coulomb explosion of the ion pair following the charge exchange process, given by

$$E_I=(q-1)\frac{e}{4\pi\epsilon X} \tag{14}$$

with X being the distance between the daughter ion $Ar^{(q-1)+}$ and the newly formed $H_2{}^+$ ion. This added energy does not cause the ions to escape radially because of confinement by the axial magnetic field.

The distance between ions X can be estimated from Langevin analysis [17,18]. Langevin found that for low-energy ion-neutral collisions, an impact parameter less than b_0 defined (in cgs units) by

$$b_0=\left[\frac{4q^2\alpha}{M_r v_r^2}\right]^{1/4} \tag{15}$$

must lead to a reaction. α is the polarizability of the neutral reactant, M_r is the reduced mass of the charge-changing partners, and v_r is the relative velocity. From this same analysis it was also found that the rate coefficient for the reaction is

$$k_L=2\pi\left[\frac{q^2\alpha}{M_r}\right]^{1/2}. \tag{16}$$

In terms of the rate coefficient, b_0 is

$$b_0 = \left[\frac{k}{\pi v_r} \right]^{1/2} . \tag{17}$$

Taking the measured rate coefficients or using Eq. (16) and $X = b_0$ the fractions f_{loss} and f_{ret} can be estimated. Assuming that ions of different charge state have the same temperature, it follows that f_{ret} will be proportional to the square root of the rate coefficient k.

Experimentally, the fraction f_{ret} was estimated by comparing numerical simulations of the ion number evolution in the ion trap with ion trap data. Two types of ion trap data were used. First, decay curves of the ion numbers were compared with numerical solutions of the coupled rate equations of the form

$$\frac{dN_i}{dt} = -k_i(\mathrm{H_2}) n_{\mathrm{H_2}} N_i + \beta_{i+1}(\mathrm{H_2}) k_{i+1}(\mathrm{H_2}) n_{\mathrm{H_2}} N_{i+1} - k_i(\mathrm{Ar}) n_{\mathrm{Ar}} N_i , \tag{18}$$

where N_i is the number of ions with charge state i, $n_{\mathrm{H_2}}$ and n_{Ar} are the Ar and H_2 densities, k_i are the charge capture rate coefficients, and β_{i+1} is the fraction f_{ret} of charge state $i+1$ that stays in the trap after capturing a single electron. Neglected is the same effect from an ion of charge state $i+1$ staying in the trap after capturing an electron from Ar, since the H_2 pressure was greater than the Ar pressure, and the charge capture rates from H_2 are larger than those from Ar.

The ion charge distribution was modified experimentally to enhance the observation of the effect of charge state $i+1$ cascading to charge state i. This was accomplished by resonantly exciting charge state i at the ω_+ frequency using a second rf generator. This increased the mean ion kinetic energy causing the ions to hit the trap electrodes and depleting the number of ions in charge state i. By making $N_{i+1} > N_i$, the term $\beta_{i+1}(\mathrm{H_2}) k_{i+1}(\mathrm{H_2}) n_{\mathrm{H_2}} N_{i+1}$ in Eq. (18) will dominate. When $N_i > N_{i+1}$ the term $-k_i(\mathrm{H_2}) n_{\mathrm{H_2}} N_i$ starts to dominate. This is shown in Fig. 6. The lines are the numerical simulations and the plotted symbols are the data.

A second method to investigate these effects is to compare the relative charge state abundances at the end of the SR pulse with the coupled rate equations of the form

$$\frac{dN_i}{dt} = \alpha_i G l n_{\mathrm{Ar}} - k_i(\mathrm{H_2}) n_{\mathrm{H_2}} N_i + \beta_{i+1} k_{i+1}(\mathrm{H_2}) n_{\mathrm{H_2}} N_{i+1} - k_i(\mathrm{Ar}) n_{\mathrm{Ar}} N_i , \tag{19}$$

where α_i is the probability of obtaining a charge state i as the result of K-shell ionization of Ar and l is the interaction length. In both methods β is adjusted so that the numerical solution fits the data. Table I shows estimates of the values of (f_{ret}) from the above analysis and compares them with the results using Eq. (12).

Preliminary analyses from the $1/\tau$ versus n plots were used to obtain the rate constants for the numerical simulation. It turned out that they were within 10% of the values found from the final full analysis. In the final analysis of the rate coefficients the experimental values of f_{ret} were used.

TABLE I. Comparison of f_{ret} as calculated from Eq. (12) and from the ion trap data. f^*_{ret} used the measured rate coefficients and $f^\dagger_{\text{ret}}$ used Eq. (16) to calculate the rate coefficients.

Charge state $i+1$ →charge state i	β_{i+1} (f_{ret})	f^*_{ret}	$f^\dagger_{\text{ret}}$
7→6	0.75	0.56	0.68
6→5	0.75	0.55	9.65
5→4	0.75	0.50	0.62
4→3	0.90	0.48	0.59

Since the accumulation of product ions did not significantly modify the Ar^{q+}-H_2 rate coefficients, this correction procedure was deemed unnecessary for the Ar^{a+}-Ar data. In an Ar^{q+}-H_2 collision, the H_2 product ion carries off nearly all of the momentum and energy liberated by the Coulomb explosion of the product ions, leaving the $Ar^{(q-1)+}$ products in the trap. In the Ar^{q+}-Ar collision, a comparable energy is equally divided between the products, significantly increasing the probability of their loss from the trap, and relatively reducing a correction to the data which the H_2 measurements show is already small.

After the fraction f_{ret} had been estimated for the H_2 measurements and the rate coefficients for Ar^{q+} on Ar measured [19], a more careful analysis was feasible. To consider the perturbing effects mentioned above, a numerical simulation of the experiment was carried out. Specifically, numerical decay curves were generated at pressures similar to those at which the actual data were taken. From these decay curves time constants τ were found and $1/\tau$ versus H_2 density plots were made. The only free parameters in the rate equations were the rate

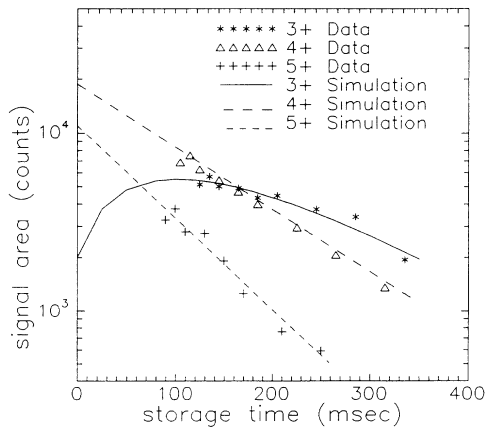

FIG. 6. Ion number vs storage time for Ar^{3+}, Ar^{4+}, and Ar^{5+}, with the Ar^{3+} number initially reduced by a factor of 10 due to excitation at ω_+. The departure from single exponential decay of Ar^{3+} becomes obvious. A numerical simulation shown by solid and dashed lines was used to estimate the fraction $\beta_{i+1}(f_{\text{ret}})$ of ions retained in the trap.

TABLE II. Rate coefficients and their errors for A^{q+} on H_2. Units are in 10^{-9} cm s^{-1}.

Ar charge state i	Uncorrected rate coefficient	Corrected rate coefficient	Statistical error	Error from β_{i+1}
3	3.5	4.3	±0.5	+0.5,−0.5
4	4.6	5.2	±0.3	+0.5,−0.5
5	5.9	5.9	±0.7	+0.3,−0.3
6	8.7	8.5	±1.2	+0.2,−0.2

coefficients, which were varied until the slope of the simulation equaled the slope of the data. At this point the simulation correctly modeled the experiment and the input rate coefficient parameters were the final rate coefficients. Equation (19) was used in the simulation during the period that the SR was pulsed through the trap. Following the SR pulse, Eq. (18) was used to simulate the storage interval.

Figure 7 shows the data and numerical simulations for Ar charge states 3, 4, 5, and 6, respectively. The data obtained from measurements of stored ion numbers versus storage time are plotted as triangles, and the solid line is the best fit to the data. The results of the simulations are plotted as circles. The intercept of the dashed line fitted through the simulation points gives the rate of ion loss with no added density of H_2 gas in the vacuum system. The ion storage rate coefficients input to the simulation, which resulted in the plotted simulation points yielding the same slope as the data, describe ion storage without ion accumulation, and are consequently interpreted as corrected ion rate coefficients. Note that the dashed line through the results of the simulation may have a negative intercept at $n(H_2)=0$. The slopes of the data and numerical simulations are the same in each figure, but the intercepts differ. This implies that the actual neutral density at the trap site differed from that plotted for the data. This residual pressure was primarily H_2, since H_2 was the dominant residual pressure measured with the RGA, and since H_2^+ signals were the largest obtained when ions formed from residual gas by electron-impact ionization were stored. The pressure was measured using a calibrated nude ion gauge, but the trap was located 40 cm away from the ion gauge, of which 27 cm were through a 2-in.-diam tube. On the other side of the trap was an additional 40 cm of 2-in.-diam tube. During the rate coefficient measurements, the only pumping was provided by a cryopump located on the six-way cross opposite the ion gauge. Since the 2-in.-diam stainless-steel tube and the trap would be outgassing mostly H_2, a pressure gra-

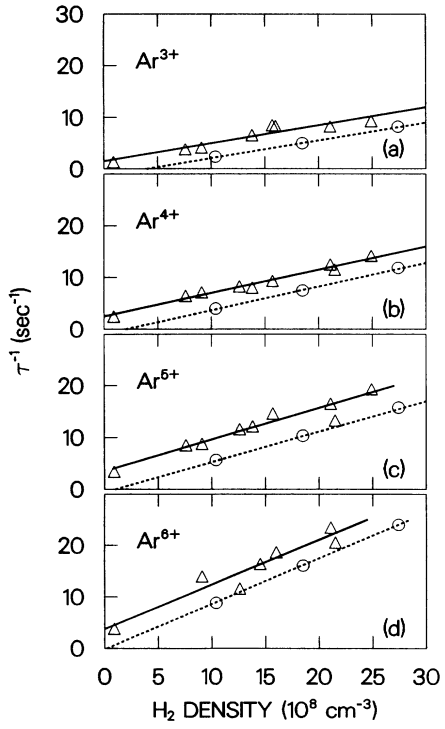

FIG. 7. Plots of τ^{-1} vs added H_2 density for (a) Ar^{3+}, (b) Ar^{4+}, (c) Ar^{5+}, and (d) Ar^{6+}. The experimental points are indicated by triangles and simulated data by circles. The slopes of the data and simulation plots yield the uncorrected rate coefficient for electron transfer.

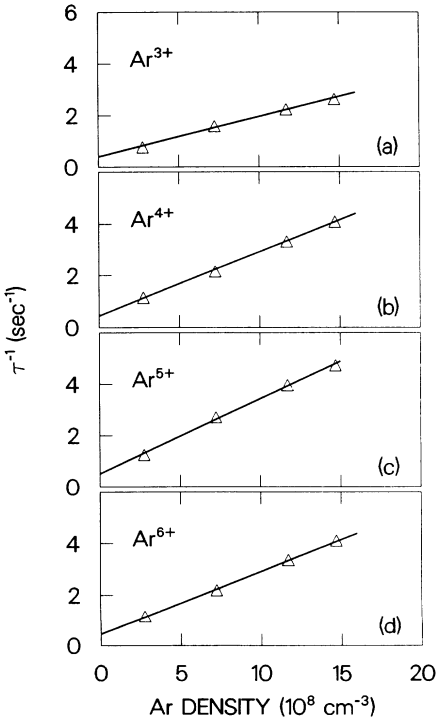

FIG. 8. Plots of experimental values of τ^{-1} (triangles) vs argon density for (a) Ar^{3+}, (b) Ar^{4+}, (c) Ar^{5+}, and (d) Ar^{6+}. The fitted slopes of the plots yield the rate coefficients.

dient down the length of the pipe resulted. Therefore the pressure at the trap would be higher than at the ion gauge. This would account for the different intercepts in the data and numerical simulations.

The differences in the y intercepts can be used to estimate the residual H_2 not taken into account in plotting the data. Taking the difference between the y intercepts $(1/\tau)$ and dividing by the rate constant yields the density. Using the ideal-gas law, the pressure was calculated. This was done for each charge state. The average value was 1.7×10^{-8} Torr, with a standard deviation of $\pm3\times10^{-9}$ Torr.

Table II lists the rate coefficients and their errors. The uncorrected rates obtained directly from the slopes of the plots are also tabulated. The errors are based on the statistical errors in the $1/\tau$ versus H_2 density plots and precise knowledge of the fractions $\beta_{i+1}(f_{\text{ret}})$.

Figure 8 shows plots of $1/\tau$ versus Ar density for Ar charge states 3–6. The rate coefficients were obtained from the fitted slopes of these plots.

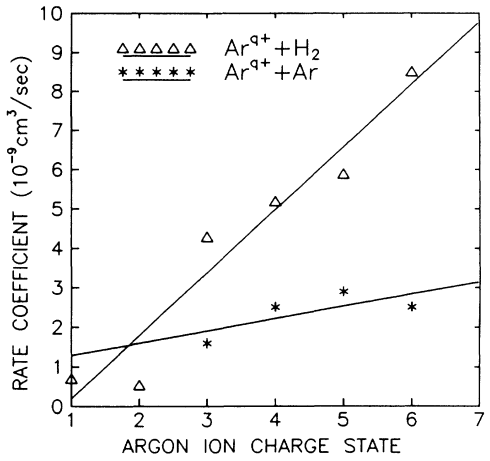

FIG. 9. Plots of rate coefficients for Ar^{q+} on H_2 and Ar vs charge state q. The solid lines are calculated Langevin rates for three collisions. Data for Ar^+ are from Ref. [24], and for Ar^{2+} from Ref. [4].

V. DISCUSSION AND CONCLUSION

There are no reported calculations of the cross sections or rate coefficients for collisions of very-low-energy argon ions with charges higher than two units, either for Ar or H_2 targets. Measurements of Ar^{q+}-Ar charge-changing cross sections have been published [20] for beam ions having energies as low as $1.8q$ keV for $3\le q\le6$. The final-state channels for double capture in the Ar^{3+}-Ar collision at 9 keV have been determined [21], and the two-electron capture cross section is near 10^{-15} cm^2 for Ar^{3+} on Ar at 30 keV [22]. The energy of these collisions is so far above those studied here that no meaningful comparison is possible. The data presented here supercedes our earlier rate coefficient measurements for Ar^{q+}-Ar electron transfer collisions $(3\le q\le5)$ which are in agreement with the present results, but had lower precision due to a significantly lower SR flux through the trap available for the earlier measurements [11]. No other data for Ar^{q+}-H_2 collisions at low energies is available for $3\le q\le6$.

The Langevin rate coefficient $k_L=2\pi qe(\alpha/\mu)^{1/2}$ scales linearly with charge state q, and is energy independent, although it is expected to apply particularly well at very low energies. Figure 9 shows that the measured rate coefficients for the Ar^{2+}-H_2 collisions, which are interpreted as single-electron capture, follow the Langevin trend closely, where $k_L=1.52q\times10^{-9}$ cm^{3}s^{-1}. The Ar^{q+}-Ar collisions also follow the Langevin trend with $k_L=0.67q\times10^{-9}$ cm^{3}s^{-1}, although more variation with charge state from the calculation is noticeable.

In summary, techniques to produce cold, stored multiply charged argon ions using focused broadband synchrotron radiation have been described, as well as measurements of the rate coefficients for electron transfer of these ions with H_2 and argon. The techniques can be applied directly to other atomic ions with K or L edges above 3 keV. For example, photoions with charges $4\le q\le11$ arising from L-shell photoionization of xenon atoms have been produced, stored, and measured. A target beam of heavy metallic atoms directed through the trap could be photoionized in a similar way. Atoms have been similarly photoionized by Compton-shifted γ rays in the expansion of SN1987A, resulting in a distribution of charge states with a temperature near 2500 K [23], providing a remarkable similarity between ions in a supernova expansion and photoions stored in a Penning ion trap. The rate coefficients for electron transfer between these ions and the dominant gases of the supernova are important in modeling the supernova plasma chemistry.

ACKNOWLEDGMENTS

Research by the collaborators from TAMU and UT/ORNL was supported by the National Science Foundation. Research by the collaborators from BNL and ANL was supported by the U.S. Department of Energy, Division of Chemical Sciences Office of Basic Energy Sciences under Contract Nos. DE-AC02-76CH00013 and W-31-109-ENG-38, respectively. M.D. was supported by a joint CNRS-NSF collaborative research grant. The Laboratoire Traitement du Signal et Instrumentation is "Unité Associée au Centre National de la Recherche Scientifque No. 842."

*Present address: Atomic Physics Laboratory, RIKEN, Wako, Saitama, 351-01, Japan.

[1] A. Dalgarno and S. E. Butler, Comments At. Mol. Phys. 7, 129 (1978).

[2] *Atomic and Molecular Processes in Controlled Thermonuclear Fusion,* edited by M. R. C. McDowell and A. M. Ferendici (Plenum, New York, 1980).

[3] S. D. Kravis, D. A. Church, B. M. Johnson, M. Meron, K.

W. Jones, J. C. Levin, I. A. Sellin, Y. Azuma, N. Berrah Mansour, H. G. Berry, and M. Druetta, Phys. Rev. Lett. **66**, 2956 (1991).
[4] S. D. Kravis, Ph.D. dissertation, Texas A&M University, 1991.
[5] J. B. Delos, Rev. Mod. Phys. **53**, 287 (1981).
[6] D. A. Church and H. M. Holzscheiter, Chem. Phys. Lett. **76**, 109 (1980).
[7] C. R. Vane, M. H. Prior, and R. Marrus, Phys. Rev. Lett. **46**, 107 (1981).
[8] M. H. Prior, R. Marrus, and C. R. Vane, Phys. Rev. A **28**, 141 (1983).
[9] H.-Y. Wang and D. A. Church, Phys. Rev. A **36**, 4261 (1987).
[10] D. A. Church and H. M. Holzscheiter, Phys. Rev. A **40**, 54 (1989).
[11] D. A. Church, S. D. Kravis, I. A. Sellin, C. S. O, J. C. Levin, R. T. Short, M. Meron, B. M. Johnson, and K. W. Jones, Phys. Rev. A **36**, 2487 (1987).
[12] F. M. Penning, Physica **3**, 837 (1936).
[13] S. D. Kravis, D. A. Church, B. M. Johnson, J. C. Levin, Y. Azuma, I. A. Sellin, M. Meron, K. W. Jones, M. Druetta, N. Mansour, H. G. Berry, and R. T. Short, Nucl. Instrum. Methods B **56/57**, 396 (1991).
[14] Fabricated by American Aspheric Co., Tucson, Arizona.
[15] B. M. Johnson, Argonne National Laboratory Report No. ANL/APS/TM-8, 1990 (unpublished), p. 200.
[16] H. G. Dehmelt, Adv. At. Mol. Phys. **3**, 53 (1967); **5**, 109 (1969).
[17] E. W. McDaniel, *Collision Phenomena in Ionized Gases* (Wiley, New York, 1964).
[18] G. Gioumousis and D. P. Stevenson, J. Chem. Phys. **29**, 294 (1958).
[19] S. D. Kravis, D. A. Church, B. M. Johnson, M. Meron, Y. Azuma, H. G. Berry, J. Levin, I. A. Sellin, and M. Druetta, in *Proceedings of the Sixteenth International Conference on the Physics of Electronic and Atomic Collisions,* AIP Conf. Proc. No. 205, edited by A. Dalgarno, R. S. Freund, M. S. Lubell, and T. B. Lucatorto (AIP, New York, 1990), p. 579.
[20] L. Liljeby, G. Astner, A. Barany, H. Cederquist, H. Danarad, S. Huldt, P. Hvelplund, A. Johnson, H. Knudsen, and K.-G. Rensfelt, Phys. Scr. **33**, 310 (1986).
[21] E. Y. Kamber, W. G. Hormis, A. G. Brenton, J. B. Hasted, and J. H. Beynon, J. Phys. B **18**, 117 (1985).
[22] H. Klinger, A. Müller, and E. Salzborn, J. Phys. **68**, 230 (1975).
[23] W. A. Mahoney, L. S. Varnell, A. S. Jacobson, J. C. Ling, R. G. Radocinski, and W. A. Wheaton, Astrophys. J. Lett. **334**, L81 (1988).
[24] E. E. Ferguson, At. Data Nuc. Data Tables **12**, 166 (1973); D. L. Albritton, *ibid.* **22**, 8 (1978).